Accepted Article

An automated quantitative image analysis tool for the identification of microtubule patterns in plants

Christine Faulkner[1,2*], Ji Zhou[1,2,3*], Alexandre Evrard[1], Gildas Bourdais[1], Dan MacLean[1], Heidrun Häweker[1], Peter Eckes[4] and Silke Robatzek[1]

[1]The Sainsbury Laboratory, Norwich Research Park, Norwich, NR4 7UH, UK

[2]Present address: John Innes Centre, Norwich Research Park, Norwich, NR4 7UH, UK

[3]Present address: Earlham Institute, Norwich Research Park, Norwich, NR4 7UH, UK

[4]Bayer AG, Crop Science Division, Industrial Park Hoechst, 65926 Frankfurt, Germany

[*]These authors contributed equally

Corresponding author:

Silke Robatzek

The Sainsbury Laboratory

Tel.: +44-1603-450-408

Fax: +44-1603-450-045

Email: robatzek@tsl.ac.uk

Running title: Image analysis of microtubule patterns

Key words: Confocal microscopy, bioimage informatics, microtubules, MAP4, TUB6, endomembrane compartments, Arabidopsis, herbicides

Abstract

High throughput confocal imaging poses challenges in the computational image analysis of complex subcellular structures such as the microtubule cytoskeleton. Here, we developed CellArchitect, an automated image analysis tool that quantifies changes to subcellular patterns illustrated by microtubule markers in plants. We screened microtubule-targeted herbicides and demonstrate that high throughput confocal imaging with integrated image

This article has been accepted for publication and undergone full peer review but has not been through the copyediting, typesetting, pagination and proofreading process, which may lead to differences between this version and the Version of Record. Please cite this article as doi: 10.1111/tra.12505

This article is protected by copyright. All rights reserved.

Accepted Article

analysis by CellArchitect can distinguish effects induced by the known herbicides indaziflam and trifluralin. The same platform was used to examine six other compounds with herbicidal activity, and at least three different effects induced by these compounds were profiled. We further show that CellArchitect can detect subcellular patterns tagged by actin and endoplasmic reticulum markers. Thus, the platform developed here can be used to automate image analysis of complex subcellular patterns for purposes such as herbicide discovery and mode of action characterisation. The capacity to use this tool to quantitatively characterise cellular responses lends itself to application across many areas of biology.

Introduction

High throughput confocal imaging using genetically encoded fluorescent markers is a powerful tool to investigate individual cell structure and function, and mechanisms that underlie subcellular responses to environmental stresses and during development. Combined with automated multiparametric image and data analysis, high throughput confocal imaging has vastly expanded the potential to screen large chemical libraries to identify molecular regulators of subcellular trafficking1. In the context of drug discovery in human studies, multiparametric data acquired from high throughput confocal imaging has proven particularly informative in understanding the dynamics of subcellular trafficking and cellular responses to bioactive chemicals[2]. Few studies have explored the application of high throughput imaging with respect to its potential to facilitate screening for bioactive chemicals that perturb (sub)cellular responses in plants[3-7]. These few imaging-based screens were designed to detect perturbations of discrete subcellular structures, i.e. the localization of fluorescent markers at the cell periphery and vesicles[8-10]. Complex subcellular structures such as the patterns tagged by microtubule and actin markers pose challenges for their analysis; current tools (e.g. FibrilTool and MicrofilamentAnalzyer) rely upon manual selection of the cells, structures or other regions of interest (ROI)[11,12]. Manual image processing prior to analysis limits automated applications, which is impractical for high content screening. Additionally, computational analysis of z-stack images from whole tissues/organisms has not yet advanced sufficiently to allow for true automation of complex subcellular structures by high throughout confocal imaging in plants.

To automate detection and analysis of complex subcellular patterns, we used an image analysis framework utilized for high-content screening. We have previously developed scripts for automated detection and quantification of discrete, spot-like (sub)cellular

This article is protected by copyright. All rights reserved.

Accepted Article

structures such as Golgi and endosomes in the cytosol, as well as plasmodesmata, pathogen-induced focal accumulations and callose deposits at the cell periphery[8-10,13]. These tools can identify and quantify structures with and without cell segmentation allowing for the potential for per cell or per image area outputs. The tools also find application beyond their intended initial use, e.g. by tracking the identified spot-like callose deposits between multiple images, CalloseMeasurer can also quantify the complex patterns of *in planta* pathogen growth[13]. An important feature of these scripts is the automated batch processing of large image data sets not requiring manual ROI selection.

Regulatory processes and the associated costs strain the delivery of new agrochemicals to the market. Part of the problem for new herbicides originates from macroscopic phenotypic screening, in which typically the primary output is plant death and does not identify subcellular targets of herbicides or herbicidal mode of action that would reduce regulatory constraints. Further, agrochemicals with more subtle but exploitable effects are not identified by such an approach. In this study we wanted to test whether the use of high throughput confocal imaging combined with automated quantitative image analysis could be used to identify subtle effects of plant subcellular responses by herbicides. We chose microtubule-targeted herbicides, most of which act via mitotic disruption by affecting microtubule polymerisation or stability. First, we addressed changes to subcellular patterns in leaf cells of plants expressing genetically encoded fluorescent microtubule markers such as GFP-MAP4 and TUB6-GFP by live imaging[14, 15]. To automatically quantify features of subcellular patterns tagged by these microtubule markers, we developed CellArchitect, a fully automated analysis pipeline that quantitatively discriminates the different effects triggered by different herbicidal compounds. Furthermore, to identify additional (side)effects by the herbicides, we screened the compounds for alterations on endomembrane compartments and correlated the screen results using statistical analysis. Quantification and classification of subcellular responses aids in predicting the mode of action for the tested herbicides and the rapid identification of their cell biological targets.

Results and discussion

Automated quantification of microtubules by CellArchitect

This article is protected by copyright. All rights reserved.

Accepted Article

To facilitate high throughput screening of microtubule-targeted herbicides, we developed the CellArchitect tool for extracting image patterns such as from microtubule markers (referred to as microtubule patterns). CellArchitect performs both cell segmentation and microtubule object detection combined with quantification. This involved sequential imaging of two cellular parameters. Microtubules were illuminated by genetically encoded fluorescent markers GFP-MAP4 and TUB6-GFP expressed in Arabidopsis. For cell definition we stained leaf tissue with propidium iodide before imaging. Images were acquired by two cameras in the Opera HCS system. Similar to our previous Acapella-based image analysis software tools[8-10, 13], CellArchitect automatically discards images from further analysis if they are out-of-focus or do not contain sufficient imaging areas or identified cells. Further, the script robustly filters background noise by intensity analysis and global adaptive thresholding. Building on our previous PDQUANT[10], we improved the identification of cell boundaries and segmentation of cells. This was applied as a first step and the cell areas thereby detected marked as regions in which to search for microtubule objects. To recognize microtubule patterns, we applied a function that smooths the image and reduces noise using a tailored 5x5 pixel Gaussian convolving kernel to reduce image noise[16]. This has the effect of relatively increasing the microtubule signal within the image at the expense of overall image detail. A local contrast-based adaptive thresholding method is then applied[17] to identify objects within the image and a binary mask of potential microtubule/non-microtubule object pixels is generated. The microtubule signals are therefore examined separately to and without noise from other image elements within every recognised cell. A topological skeletonization method[18] was applied to extract 1D skeleton lines from the microtubule masks by identifying the line within the shape equidistant from each boundary. The extracted skeleton is then further examined with a 4-connected Von Neumann neighbourhood method[19] and fluorescence intensity values in order to identify continuous chains of skeleton pixels that have another microtubule pixel in each direction horizontally and vertically (but not diagonally). Thus, discrete chains within the skeleton are considered to be objects within the overall set of skeletons. The objects within the skeleton are finally selected and measured. Skeleton objects are classified on the basis of object length (Figure S1). CellArchitect produces accurate measurements of microtubule patterns in Arabidopsis epidermal pavement cells, and provides a platform for quantification of microtubule object features (Figures S1 and S2).

This article is protected by copyright. All rights reserved.

Accepted Article

For assessing the broader utility of CellArchitect, we tested this image pattern recognition tool on plant cells in which actin was visualized by genetically encoded ABD2-GFP[20], as well as cells in which the endoplasmic reticulum (ER) was marked by genetically encoded GFP-HDEL[21] in Arabidopsis. CellArchitect was able to detect both subcellular patterns (Figure S3). Representation of the tubular ER network suggests that with the definition of biologically relevant, measurable parameters, CellArchitect could be exploited in quantitative analysis of ER structure.

Quantification of microtubule patterns induced by known herbicides

We applied high throughput confocal imaging integrating computational image analysis using CellArchitect to profile altered microtubule patterns in herbicide-treated Arabidopsis epidermal pavement cells, with the aim to predict the biological process each herbicide targets. To validate our protocol, we first examined the known herbicides oryzalin, trifluralin and indaziflam for distinct effects on the microtubule cytoskeleton compared with control data (DMSO treatment). Images from replicate treatments were processed with CellArchitect to quantify the following features: object density per cell, relative population of object length categories and object width (Figure 1). Object density was expected to quantify a total reduction in objects of microtubule patterns per cell, that would be expected to infer on microtubule depolymerisation or bundling. Object length categorisation quantifies the number of microtubule objects in each of the short, medium and long size classes. These categories were selected based on overall distribution of microtubule object length (Figure S1). The total length (in pixels) of objects in a given category is expressed as a proportion of the total length of detected objects within a given cell such that pattern changes arising from microtubule fragmentation can be quantified. Increased object thickness or width represents a pattern feature that would be expected to infer on microtubule bundling.

Qualitative assessment of oryzalin treatment showed strong effects on microtubules (Figure 2), in agreement that oryzalin prevents microtubule polymerisation and thus making extend microtubules more likely to depolymerize[22]. Trifluralin treatment also reduced the number and length of microtubules in a cell, while indaziflam treatment has little to no effect (Figure 2). High throughput imaging and CellArchitect analysis quantified the objects of microtubule patterns for each treatment and confirmed that oryzalin treatment increased the relative number of objects in the short class size for both, the GFP-MAP4 and the TUB6-GFP marker (Figure 3). Consistently, the relative number of GFP-MAP4 and TUB6-GFP tagged objects in

This article is protected by copyright. All rights reserved.

Accepted Article

the long class size decreased in oryzalin treatments. This indicates that oryzalin effects are proportional to the total population of microtubule objects; the density of objects decreased significantly indicating depolymerisation and/or bundling also occurred. For both trifluralin and indaziflam, the relative number of microtubule objects in the short size class was similar for the GFP-MAP4 marker. The difference in the appearance of the patterns is accounted for by the significant difference in object density induced by trifluralin but not indaziflam. Short size microtubule objects marked by TUB6-GFP were marginally increased in trifluralin treatments, which was correlated with reduced microtubule objects in the long size class, and a similar effect was also detected with the GFP-MAP4 marker.

Quantification of object density for both GFP-MAP4 and TUB6-GFP microtubule markers revealed similar effects of oryzalin and trifluralin. Both herbicides induced a significant reduction in microtubule objects per cell (Figure 3). This correlated with an increase in object width. By contrast, indaziflam treatment induced no change to either object density per cell or object width. Oryzalin and trifluralin are synthetic compounds of the dinitroaniline group, which bind to the α-subunit of tubulin, disassembling microtubules[22]. This mode of action is in agreement with our results measuring the relative proportion of short and long microtubule objects. In addition, object width measurement suggests the possibility that oryzalin and trifluralin induce bundling, an effect imperceptible in visual assessment of our microscopy images. In contrast to oryzalin and trifluralin, the herbicide indaziflam acts as cellulose biosynthesis inhibitor[23], and in agreement we found no or little effects of indaziflam on objects of microtubule patterns. It can however decrease the co-localization of cellulose synthase and microtubules, suggesting a potential indirect effect on microtubule patterns, consistent with our findings on slightly decreased long class objects marked by TUB6-GFP (Figure 3). Together, these results demonstrate that CellArchitect enables the quantification of distinct microtubule patterns and is therefore suited to screening chemical libraries for distinct herbicidal activities.

Quantification of microtubule patterns induced by compounds with herbicidal activity

Known classes of herbicides have been reinforced by newer compounds with the aim to overcome resistances attributable to isotope specific differences of their targets in taxonomic groups. This is traditionally achieved by high throughput screening of natural product and synthetic compound libraries for herbicidal activities, measured as plant death specific to certain taxonomic groups. To gain insights into the mode of action of compounds identified

This article is protected by copyright. All rights reserved.

Accepted Article

from such screens, we examined six compounds with known herbicidal activity but undescribed effects on the microtubule cytoskeleton. Compounds (C) 1-6 all induced fragmentation of microtubules when compared to control treatments (Figure 4). Quantitative analysis using CellArchitect revealed decreased object density, measured for both GFP-MAP4 and TUB6-GFP markers, for C1-6 indicating that each compound induced a degree of microtubule depolymerisation (Figure 3). Each compound also induced a measurable increase in object width for GFP-MAP4 tagged microtubules, suggesting bundling. The trend in these measurements was replicated in TUB6-GFP tagged objects. Comparison of the relative abundance of microtubule objects of different sizes suggest that C1-6 each induced fragmentation, as evidenced from the decreased proportion of long objects while the proportion of short objects increased. This is most severe for C4-6. C4, C5 and C6 are visually and quantifiably indistinguishable in effect, each causing severe microtubule fragmentation.

Qualitative differences in the compound effects were apparent (Figure 4), suggesting vastly different effects of C1 and both C2 and C3. C1 induced curled and fragmented objects indicative of microtubule nucleation while C2 and C3 both produced 'shard-like' objects suggesting bundling of microtubules. Quantitative analysis of the effects of C1, C2 and C3 by CellArchitect separates all three compounds when considering object density (Figure 3). This is represented by the measurable increase in object width - C2 and C3 can be grouped, and separated from the remaining compounds, with respect to object width. The 'shard-like' objects induced by C2 and C3 are reminiscent of microtubule patterns observed upon interference with katanin function required for severing (24). Based on these similarities it is possible to hypothesize that the biological process targeted by C2 and C3 may involve katanin-mediated severing.

Our results show that the six tested compounds belong to the group of microtubule-targeted herbicides. Compared with microtubule patterns induced by oryzalin, compound C2 was most similar, including object length (short and long class), density, and width. C1 produced also similar patterns for object length with a similar trend for object density and width. It is possible to speculate that C1 and C2 exhibit a mode of action similar to oryzalin. By contrast, C4, C5, and C6 all showed much stronger effects on object length (more short and less long class objects) compared with oryzalin, while showing lesser effect on object density and width. Also, microtubule patterns induced by C4, C5 and C6 were distinct to those produced by trifluralin. This suggests that C4, C5, C6 act as compounds causing microtubule

This article is protected by copyright. All rights reserved.

Accepted Article

disassembly likely through a distinct mode of action than the dinitroaniline herbicides oryzalin and trifluralin. However, despite differences in chemical structures and effects on microtubule patterns, the microtubule-targeted compounds usually associate with one of the three tubulin binding sites changing the confirmation of the tubulin molecule, thereby preventing polymerization[22].

Quantification of herbicide-treated endomembrane compartments

The quantification of microtubule patterns revealed indistinguishable effects by C4-6. Microtubules are linked with the localization of cellulose synthase, another herbicidal target and a cargo of the endomembrane trafficking system[22, 25]. Therefore, to identify additional (side)effects by the herbicides that could further differentiate their mode of activity, we applied high throughput confocal imaging integrating computational image analysis by EndomembraneQuantifier[9], and profiled the effect of each herbicide on endomembrane compartment subcellular structures. These included endosomes, the *trans*-Golgi network (TGN) and Golgi bodies, visualized by the well-established genetically encoded RFP-ARA7, VTI12-YFP, SYP32-YFP markers, respectively[26]. Effects on these endomembrane compartments by all tested compounds were subtle and imperceptible to the human eye without quantification. With respect to C4-6, C4 exhibited the strongest effects (Figure 5). Statistical analysis suggests that C4 induced an increase in endosome size correlated with a decrease in endosomal numbers relative to DMSO control. Both C4 and C6 perturbed the number of TGN compartments, while C5 specifically affected the size of Golgi compartments. These results indicate differences between C4 and C6 compared to C5. Correlation of these effects with their structures reveals that C5 is specified by a chlorobenzene group while C4 and C6 have a fluorobenzene group (2-fluorobenzene for C4 and 1,5-difluorobenzene for C6; Figure S4). Thus, it is possible that microtubule effects are induced by the common backbone of the compound while the halide benzene group has additional differential effects on endomembrane compartments. Interestingly, indaziflam treatment reduced the number of Golgi compartments relative to DMSO control (Figure 5), broadening its effect from cellulose biosynthesis inhibition to generally altering secretory trafficking.

In our study, we show the strength and advantages of quantitative multiparametric image analysis to measure subcellular patterns. This method enables the identification of modes of action of compounds in the process of herbicide discovery. We have developed CellArchitect,

This article is protected by copyright. All rights reserved.

Accepted Article

an Acapella-based automated image analysis tool that batch processes images from high throughput confocal microscopy of genetically encoded microtubule markers expressed in Arabidopsis. In particular, CellArchitect performs feature-based extraction, quantifying microtubule patterns according to features relating to object length, width and density. We have demonstrated that these quantitative features differentiate between the effects of the tested herbicidal compounds on microtubule patterns. While CellArchitect quantifies image patterns and extracts image features, it only provides indirect estimates of microfilament organization, which are better estimated using FibrilTool and Microfilament Analyzer[11, 12]. Both software tools are excellent for investigating microtubule organization: 1) FibrilTool is developed as ImageJ plug-in and quantifies the anisotropy of fiber arrays and their cellular orientation[11], and 2) Microfilament Analyzer is a software package for detecting the filamentous structures and their orientation in root epidermal cells[12]. Given that FibrilTool and Microfilament Analyzer require manual inputs e.g. to select a ROI, while this enables analysis of microfilaments, it makes the image processing of microtubule patterns time consuming and not applicable for batch processing. To automate image processing, we chose to detect and quantify microtubule patterns on a projection of the z-stack because it simplifies the processing considerably. Thus, CellArchitect provides a complementary software solution that automates the image processing step and not requiring manual selection of an ROI, making it a software tool suited for large screening of e.g. chemical libraries or mutant populations.

As a testament, CellArchitect could differentiate between C1, C2, C3, and C4-C6 without any human intervention in the analysis. In combination with EndomembraneQuantifier, automated analysis could discriminate further between C4, C5 and C6 in patterns. This shows that these tools may be combined to identify the subcellular location of herbicidal targets, with applications in both agrochemical and research contexts. Beyond the quantification demonstrated here, CellArchitect carries the potential to extract additional features such as object fluorescence intensity and orientation, recognises other subcellular patterns such as those tagged by actin and ER markers. Thus, this tool may be widely exploited for the fully automated analysis of subcellular patterns of different markers. In conclusion, we have established an automated image analysis tool for complex subcellular patterns that facilitates high throughput confocal imaging. This creates the potential for image-based screenings, such as the patterns tagged by cytoskeleton markers, in the discovery process of herbicide

This article is protected by copyright. All rights reserved.

Accepted Article

identification, as well as the application of rigorous quantitative methods for cellular responses in plant biology.

Materials and Methods

Plant material

Plant material was *Arabidopsis thaliana*, of the Col-0 ecotype unless otherwise indicated. Marker lines used in the study were 35S::GFP-MAP4 (microtubule marker, in Ler ecotype,[14]); 35S::TUB6-GFP (microtubule marker, beta-tubulin6-GFP); pUBQ10::mRFP-ARA7/RabF2b (endosome marker, provided by K. Schumacher, Heidelberg, Germany); pUBQ10::VTI12-YFP (*trans*-Golgi network marker[26]); pUBQ10::SYP32-YFP (Golgi marker[26]); 35S::GFP-FABD2 (actin marker[20]) and 35S::GFP-HDEL (ER marker[21]). Arabidopsis seedlings were grown on soil for 14 days in 12 h light and 60% humidity.

Chemical treatments

Cotyledons were detached from seedlings and incubated in 25 μM solutions (0.25% DMSO) of the respective compounds. Controls were incubated in 0.25% DMSO. Cotyledons were vacuum infiltrated for 2 min so that treatment solutions penetrated the tissue and then incubated at room temperature for 4 hrs. For microtubule labelled lines, 10 min prior to imaging propidium iodide was added to the solution to a final concentration of 100 μg/mL.

Cotyledons were imaged by the Opera HCS microscope as described by Beck et al.[9]. In brief, leaves were secured on rubber tipped stamps and upended in glass bottom 96 well plates. Imaging was performed with 40x water immersion objective (0.9 NA) with an x-y optical resolution of 0.26 nm (measured at 500 nm). GFP was excited by 488nm laser and emission captured with the 540/75 band-pass filter. RFP and propidium iodide were excited with the 561nm laser and collected with the 600/40 band-pass filter. The exposure was varied dependent on marker line in the range 40-120 ms. For z-stacks, 21 images with a resolution of 681 x 486 pixels were collected at 1 μm intervals. For single channel imaging, 6 z-stacks per leaf were collected. For dual channel imaging 3 z-stacks per leaf were collected. 3-6 leaves per treatment were imaged within a replicate experiment, and for each experiment 3 independent replicates were performed.

This article is protected by copyright. All rights reserved.

Accepted Article

Image analysis

CellArchitect is an Acapella-based image analysis tool that provides an automated workflow to detect and quantify patterns from plant bioimages. Broadly, it proceeds by identifying leaf epidermal cells of interest, performs detection of objects labelled by fluorescent-tagged cytoskeleton markers, and extracts features for quantifying cytoskeleton objects. To make CellArchitect suited for batch processing of bioimages taken from whole leaves, an uneven organ, we included a pre-processing step to calibrate Opera confocal microscopy images, then to generate maximum projections from optical z-planes and excluding maximum projections containing out-of-focus areas, thus not valid for pattern analysis (Figure 1). To this end, a maximum intensity projection is used to reconstruct optical z-planes captured by the two cameras of the Opera microscope. After that, CellArchitect applies fluorescence intensity histogram equalisation to calibrate the projected images so that batch processing could be carried out on maximum projections with similar fluorescence intensity histograms[27]. The intensity histogram is spread across the most frequent fluorescence intensity values of a maximum projection and then equalised to ensure that the intensity histogram of the maximum projection presents a roughly linear cumulative distribution function (rescaled to include all intensities that fall within the 2nd and 98th percentiles). To identify out-of-focus areas and valid focus areas of the maximum projections, CellArchitect applies a dynamic thresholding value based on signals captured by camera one. The value of the threshold is taken to be 75% of the computed whole maximum projection image Otsu thresholding value. Regions with low fluorescence intensity values (out-of-focus areas, below the threshold) and regions with high intensity and contrast values (valid focus areas, equal or above the threshold) are identified[28]. Background pixels are removed if they are lower than the thresholding value. Finally, a cell segmentation process[10] is used to extract the pavement cell outlines as well as signals from stomata. In this step, CellArchitect applies an adaptive Gaussian thresholding method – a tailored 5x5 Gaussian convolving kernel [1,4,16,4,1; 4,16,32,16,4; 16,32,128,32,16; 4,16,32,16,4; 1,4,16,4,1] to smooth and reduce image noise before thresholding[16]. The previously identified out-of-focus areas, the pavement cell outlines and stomata objects, are masked (Figure 1), and the resulting processed maximum projection images contain pavement cells that are considered valid for microtubule pattern detection. In a next step, CellArchitect removes pavement cells with sizes and width-to-length ratio above the 98th percentile (too big) or below the 2nd percentile (too small) from the maximum projection images. The remaining pavement cells of the maximum projection image are then analysed for signals captured by camera two, the microtubule patterns, and only kept with

This article is protected by copyright. All rights reserved.

Accepted Article

median pixel intensities. If the algorithm retains at least two pavement cells per maximum projection image at this step, further analysis of the microtubule patterns will be triggered.

For microtubule pattern analysis, the signals captured by camera two, CellArchitect applies a tailored 5x5 Gaussian convolving kernel [1,4,16,4,1; 4,16,32,16,4; 16,32,128,32,16; 4,16,32,16,4; 1,4,16,4,1] to smooth and reduce image noise. As microtubule pattern signals can be unevenly distributed amongst identified pavement cells, the algorithm processes the signals from camera two of the maximum projections through a local contrast-based adaptive thresholding method from the Acapella framework. Pixels are retained if their fluorescence intensity values are higher than the 65th percentile of the intensity distribution in a given image object, e.g. a detected pavement cell or a microtubule object. The algorithm then applies a pattern recognition process generating binary masks of microtubule objects based on per-object thresholding. Briefly this uses the 4-connected Von Neumann neighbourhood method[19] available from the Acapella framework to determine skeleton pixels that touch another pixel's edges, either horizontally or vertically. Such pixels are considered connected and therefore part of the same microtubule object. Next, CellArchitect applies a "corner-connected" fluorescence intensity approach, comparing the intensity values of previously connected pixels retaining only connected pixels with the 35% highest intensity values. The next step is to extract skeleton lines from the connected pixels, generating a 1-pixel wide mask of skeleton objects, again with the skeleton method available from the Acapella framework. As fluorescence intensities of pixels from z-planes of deeper layers inside the leaf are generally lower than those from higher layers, this breaks artefactual microtubule grid-like patterns caused by the maximum projection and retains planar microtubule structures. By relying on natural spatial distinctions in the microtubule network our approach balances speed of execution with the inhibitory computational complexity of fully deconvoluting a large connected skeleton.

The length of a microtubule object is then calculated based on the skeleton mask of connected pixels and between two end point skeleton pixels. An average width for each object is calculated by dividing the objects area (the total number of pixels contained within the object), by the number of skeleton pixels (the total pixels along the medial axis of the object). This method assumes that objects are of essentially constant width along the entire length. It should be noted that width measurements can only be used as an indicator of structural change as microtubule width is approximately 10 times smaller than the limits of

This article is protected by copyright. All rights reserved.

Accepted Article

resolution of the confocal imaging system. With aims of providing a speedy approach to visualise changes of microtubule patterns triggered by different chemicals, CellArchitect classifies and colour codes the microtubule skeleton objects based on their length values (Figure S1), and sorts them into an object list so that microtubule objects are extracted, covering shard-shape to linear, filamentous patterns. CellArchitect calculates microtubule object density per cell (0-100%) based on the coverage of detected microtubule objects in a given pavement cell divided by the area of the cell. Microtubule object intensity (0-128) is determined based on the median fluorescence intensity value of all microtubule signals enclosed in a given pavement cell. Quantifiable results generated by CellArchitect are saved in two files, one containing results for every processed maximum projection image and one for overall results. The Acapella source code of CellArchitect is freely available at https://github.com/TeamMacLean/CellArchitect.

Maximum projection images for microtubule patterns and endomembrane compartments were analysed with CellArchitect and EndomembraneQuantifier[9] respectively. Quantification results were saved in CSV files including experimental metadata such as image name, treatment, experiment date, and other related phenotypic outputs. Experimental values for object number were normalised against the average of the control.

Manual detection of microtubule patterns was performed on maximum intensity projections using Fiji tools[29]. Pavement cell outlines were manually determined as ROI using a polygon selection, prior manual adjustment of brightness and contrast. After that, a manual thresholding of the image was applied to capture the microtubule objects, which were then measured using the skeleton analysis tool. Manual measurements of the overall detected object length were compared to measurements by CellArchitect.

Statistical Analysis

Analysis of variance and post-hoc Tukey (HSD) tests are used to detect significant differences between the chemicals. Different letters indicate significant differences between chemicals, calculated for each parameter separately ($p<0.05$). All statistics are performed using R (R Development Core Team, 2008; http://www.R-project.org) and the packages agricolae[30] and multcomp[31].

Acknowledgements

This article is protected by copyright. All rights reserved.

We like to thank members of the Robatzek laboratory for fruitful discussions. This research was supported by Bayer Crop Science (P.E., S.R.), the Gatsby Charitable Foundation (D.M., S.R.) and the European Research Council (S.R.).

Accepted Article

This article is protected by copyright. All rights reserved.

Accepted Article

Supporting Information

Figure S1: Overall population analysis of microtubule objects. (A) Boxplot representing the overall population of microtubule objects (blue dots) detected by CellArchitect in control treated Arabidopsis cotyledons. Data show the results of one representative image. The plotted box indicates the boundaries of the upper and lower quartiles with bars indicating maximum and minimum values, the bold black bar identifies the median, and the dashed lines indicate the selected boundaries classified as short, medium, and long microtubule objects. (B) Density plot representing the proportion (y-axis) of the microtubule object lengths (x-axis) detected by CellArchitect in Arabidopsis cotyledons treated with mock (DMSO), C2 and C5. Data show the results of one representative image for each treatment revealing that the proportion of short microtubule objects is higher in C2 and C5 compared to DMSO.

Figure S2: Comparison of microtubule objects measured per cell using CellArchitect and manual measurement. No significant differences were observed between the two methods using a Student t-test, neither in control conditions ($p = 0.81$, $n = 11$) nor after herbicide treatment ($p = 0.86$, $n = 13$). The overall % of variation between the two methods is 15.9% (+/- 11.7%).

Figure S3: Detection of microtubule patterns tagged by GFP-MAP4, actin patterns tagged by GFP-FABD2 and endoplasmic reticulum patterns tagged by GFP-HDEL in Arabidopsis cotyledons using CellArchitect. Scale bars are 25 µm.

Figure S4: Chemical structures for C4, C5 and C6.

CellArchitect algorithm: https://github.com/TeamMacLean/CellArchitect

This article is protected by copyright. All rights reserved.

Accepted Article

References

1. Collinet C, Stöter M, Bradshaw CR, Samusik N, Rink JC, Kenski D, Habermann B, Buchholz F, Henschel R, Mueller MS, Nagel WE, Fava E, Kalaidzidis Y, Zerial M. Systems survey of endocytosis by multiparametric image analysis. *Nature.* 2010;464(7286):243-9. https://doi.org/10.1038/nature08779.

2. Warchal SJ, Unciti-Broceta A, Carragher NO. Next-generation phenotypic screening. *Future Med Chem*. 2016;8(11):1331-47. https://doi.org/10.4155/fmc-2016-0025.

3. Robert S, Chary SN, Drakakaki G, Li S, Yang Z, Raikhel NV, Hicks GR. Endosidin1 defines a compartment involved in endocytosis of the brassinosteroid receptor BRI1 and the auxin transporters PIN2 and AUX1. *Proc Natl Acad Sci USA*. 2008;105(24):8464-9. https://doi.org/10.1073/pnas.0711650105.

4. Drakakaki G, Robert S, Szatmari AM, Brown MQ, Nagawa S, Van Damme D, Leonard M, Yang Z, Girke T, Schmid SL, Russinova E, Friml J, Raikhel NV, Hicks GR. Clusters of bioactive compounds target dynamic endomembrane networks in vivo. *Proc Natl Acad Sci USA*. 2011;108(43):17850-5. https://doi.org/10.1073/pnas.1108581108.

5. Codreanu MC, Audenaert D, Nguyen L, Beeckman T, Russinova E. Small-molecule dissection of brassinosteroid signaling. *Methods Mol Biol*. 2012;876:95-106. https://doi.org/10.1007/978-1-61779-809-2_7.

6. Doyle SM, Haeger A, Vain T, Rigal A, Viotti C, Łangowska M, Ma Q, Friml J, Raikhel NV, Hicks GR, Robert S. An early secretory pathway mediated by GNOM-LIKE 1 and GNOM is essential for basal polarity establishment in Arabidopsis thaliana. *Proc Natl Acad Sci USA*. 2015;112(7):E806-15. https://doi.org/10.1073/pnas.1424856112.

7. Zhang C, Brown MQ, van de Ven W, Zhang ZM, Wu B, Young MC, Synek L, Borchardt D, Harrison R, Pan S, Luo N, Huang YM, Ghang YJ, Ung N, Li R, Isley J, Morikis D, Song J, Guo W, Hooley RJ, Chang CE, Yang Z, Zarsky V, Muday GK, Hicks GR, Raikhel NV. Endosidin2 targets conserved exocyst complex subunit EXO70 to inhibit exocytosis. *Proc Natl Acad Sci USA*. 2016;113(1):E41-50. https://doi.org/10.1073/pnas.1521248112.

This article is protected by copyright. All rights reserved.

Accepted Article

8. Salomon S, Grunewald D, Stüber K, Schaaf S, MacLean D, Schulze-Lefert P, Robatzek S. High-throughput confocal imaging of intact live tissue enables quantification of membrane trafficking in Arabidopsis. *Plant Physiol*. 2010;154(3):1096-104. https://doi.org/10.1104/pp.110.160325.

9. Beck M, Zhou J, Faulkner C, MacLean D, Robatzek S. Spatio-temporal cellular dynamics of the Arabidopsis flagellin receptor reveal activation status-dependent endosomal sorting. *Plant Cell*. 2012;24(10):4205-19. https://doi.org/10.1105/tpc.112.100263.

10. Fitzgibbon J, Beck M, Zhou J, Faulkner C, Robatzek S, Oparka K. A developmental framework for complex plasmodesmata formation revealed by large-scale imaging of the Arabidopsis leaf epidermis. *Plant Cell*. 2013;25(1):57-70. https://doi.org/10.1105/tpc.112.105890.

11. Boudaoud A, Burian A, Borowska-Wykręt D, Uyttewaal M, Wrzalik R, Kwiatkowska D, Hamant O. FibrilTool, an ImageJ plug-in to quantify fibrillar structures in raw microscopy images. *Nat Protoc*. 2014;9(2):457-63. https://doi.org/10.1038/nprot.2014.024.

12. Tsugawa S, Hervieux N, Hamant O, Boudaoud A, Smith RS, Li CB, Komatsuzaki T. Extracting Subcellular Fibrillar Alignment with Error Estimation: Application to Microtubules. *Biophys J*. 2016;110(8):1836-44. https://doi.org/10.1016/j.bpj.2016.03.011.

13. Zhou J, Spallek T, Faulkner C, Robatzek S. CalloseMeasurer: a novel software solution to measure callose deposition and recognise spreading callose patterns. *Plant Methods*. 2012;8(1):49. https://doi.org/10.1186/1746-4811-8-49.

14. Marc J, Granger CL, Brincat J, Fisher DD, Kao Th, McCubbin AG, Cyr RJ. A GFP-MAP4 reporter gene for visualizing cortical microtubule rearrangements in living epidermal cells. *Plant Cell*. 1998;10(11):1927-40. https://doi.org/10.1105/tpc.10.11.1927.

15. Nakamura M, Naoi K, Shoji T, Hashimoto T. Low concentrations of propyzamide and oryzalin alter microtubule dynamics in Arabidopsis epidermal cells. *Plant Cell Physiol*. 2004;45(9):1330-4. https://doi.org/10.1093/pcp/pch300.

This article is protected by copyright. All rights reserved.

Accepted Article

16. Knutsson H, Westin C. Normalized and Differential Convolution: Methods for Interpolation and Filtering of Incomplete and Uncertain data. *Proceedings of IEEE Computer Society Conference on Computer Vision and Pattern Recognition. New York City, USA. IEEE*. 1993;515–523. https://doi.org/10.1109/CVPR.1993.341081.

17. Sezgin M, Sankur B. Survey over image thresholding techniques and quantitative performance evaluation. *J Electron Imaging*. 2004;13(1):146–165. http://dx.doi.org/10.1117/1.1631315.

18. Gonzalez RC, Woods RE, Masters BR. Digital Image Processing. 3rd Editio. *USA: Pearson Education - Prentice Hall*. 2008. https://doi.org/10.1117/1.3115362.

19. Brummitt C. Packard Snowflakes on the von Neumann Neighborhood. *J Cell Autom*. 2008;3(1):57–79.

20. Voigt B, Timmers ACJ, Samaj J, Muller J, Baluska F, Menzel D. GFP-ABD2 fusion construct allows in vivo visualization of the dynamic actin cytoskeleton in all cells of Arabidopsis seedlings. *Eur J Cell Biol*. 2005;84(6):595-608. https://doi.org/10.1016/j.ejcb.2004.11.011.

21. Brandizzi F, Hanton S, DaSilva LL, Boevink P, Evans D, Oparka K, Denecke J, Hawes C. ER quality control can lead to retrograde transport from the ER lumen to the cytosol and the nucleoplasm in plants. *Plant J*. 2003;34(3):269-281. https://doi.org/10.1046/j.1365-313X.2003.01728.x.

22. Dostál V, Libusová L. Microtubule drugs: action, selectivity, and resistance across the kingdoms of life. *Protoplasma*. 2014;251(5):991-1005. https://doi.org/10.1007/s00709-014-0633-0.

23. Brabham C, Lei L, Gu Y, Stork J, Barrett M, DeBolt S. Indaziflam herbicidal action: a potent cellulose biosynthesis inhibitor. *Plant Physiol*. 2014;166(3):1177-1185. https://doi.org/10.1104/pp.114.241950

This article is protected by copyright. All rights reserved.

Accepted Article

24. Stoppin-Mellet V, Gaillard J, Vantard M. Katanin's severing activity favors bundling of cortical microtubules in plants. *Plant J*. 2006;46(6):1009-1017. https://doi.org/10.1111/j.1365-313X.2006.02761.x.

25. Li S, Lei L, Somerville CR, Gu Y. Cellulose synthase interactive protein 1 (CSI1) links microtubules and cellulose synthase complexes. *Proc Natl Acad Sci USA*. 2012;109(1):185-190. https://doi.org/10.1073/pnas.1118560109.

26. Geldner N, Dénervaud-Tendon V, Hyman DL, Mayer U, Stierhof YD, Chory J. Rapid, combinatorial analysis of membrane compartments in intact plants with a multicolor marker set. *Plant J*. 2009;59(1):169-178. https://doi.org/10.1111/j.1365-313X.2009.03851.x.

27. Kapur J, Sahoo P, Wong A. A new method for gray-level picture thresholding using the entropy of the histogram. *Comput Vision, Graph Image Process*. 1985;29(3):273–285. https://doi.org/10.1016/0734-189X(85)90125-2.

28. Otsu N. A threshold selection method from gray-level histograms. *IEEE Trans Syst Man Cybern*. 1979;9(1):62–66. https://doi.org/10.1109/TSMC.1979.4310076.

29. Schindelin J, Arganda-Carreras I, Frise E, Kaynig V, LongairM, Pietzsch T, Preibisch S, Rueden S, Saalfeld S, Schmid B, Tinevez J-Y, White DJ, Hartenstein V, Eliceiri K, Tomancak P, Cardona A. Fiji: an open-source platform for biological-image analysis. *Nature Methods*. 2012;9(7):676-682. https://doi.org/10.1038/nmeth.2019.

30. De Mendiburu F. Agricolae: Statistical procedures for agricultural research using R(Online). 2016. Available at http://tarwi. lamolina. edu. pe/˜fmendiburu/.

31. Hothorn T, Bretz F, Westfall P. Simultaneous inference in general parametric models. *Biom J*. 2008; 50(3):346-363. https://doi.org/10.1002/bimj.200810425.

This article is protected by copyright. All rights reserved.

Accepted Article

Figure Legends

Figure 1: The CellArchitect analysis workflow. 1. The users loads image files. 2. Camera one captures cell outlines, which are used for cell segmentation. Recognized cell regions are retained in the analysis. 3. Camera two acquires microtubule signals and CellArchitect applies pattern recognition and feature-based extraction to 4. quantify microtubule objects in every recognized cell region.

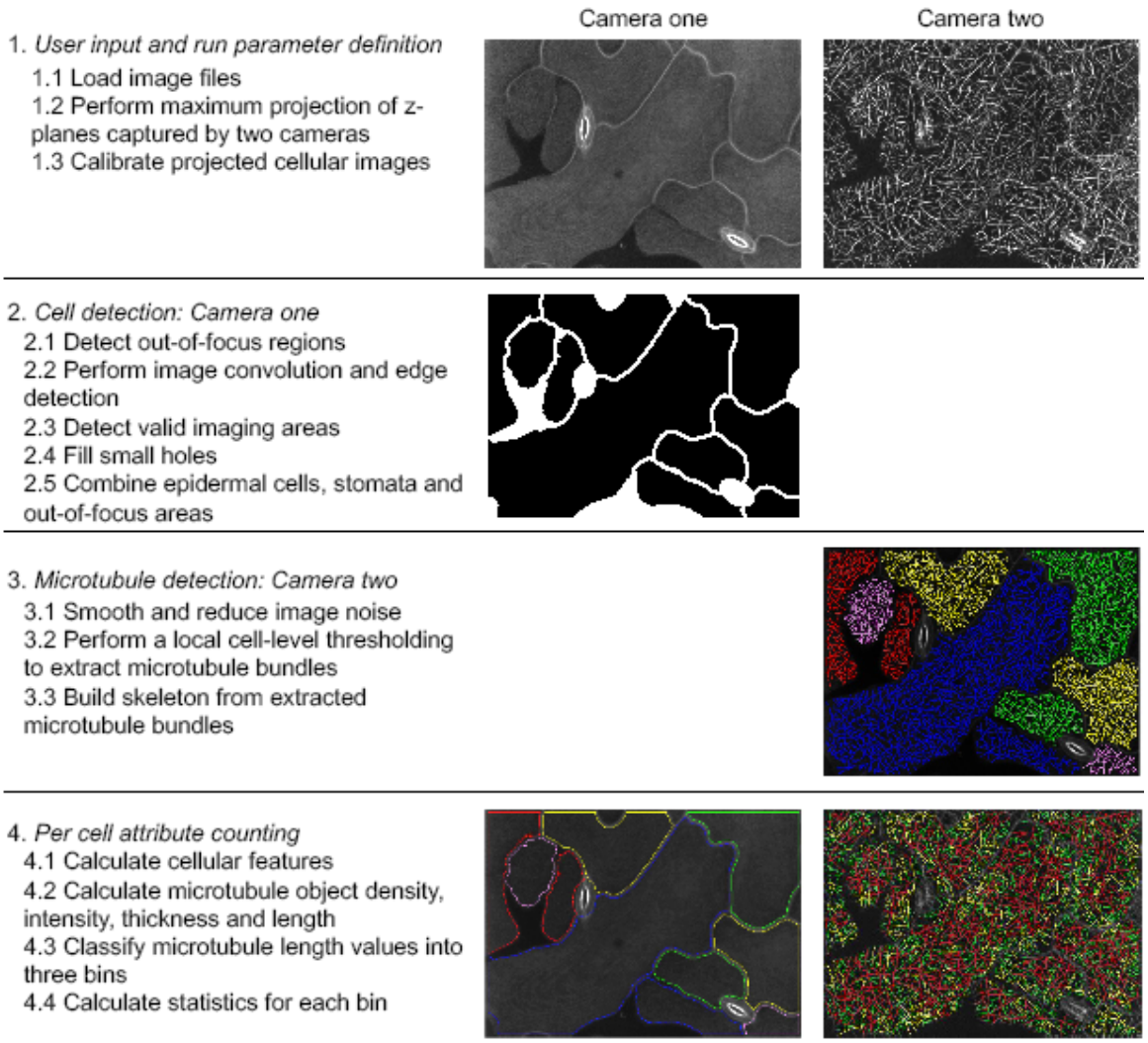

Figure 2: The effects of known herbicides oryzalin (Ory), indaziflam (Ind) and trifluoralin (Tri) on microtubules of Arabidopsis cotyledon epidermal pavement cells. Control treatment is 0.25% DMSO. Microtubules are marked by stable expression of GFP-MAP4 and TUB6-GFP. Microtubule pattern detection by CellArchitect is shown with colour coding according

This article is protected by copyright. All rights reserved.

Accepted Article

to object length: green: short; yellow: medium-short; orange: medium-long; red: long. Scale bars are 15 µm.

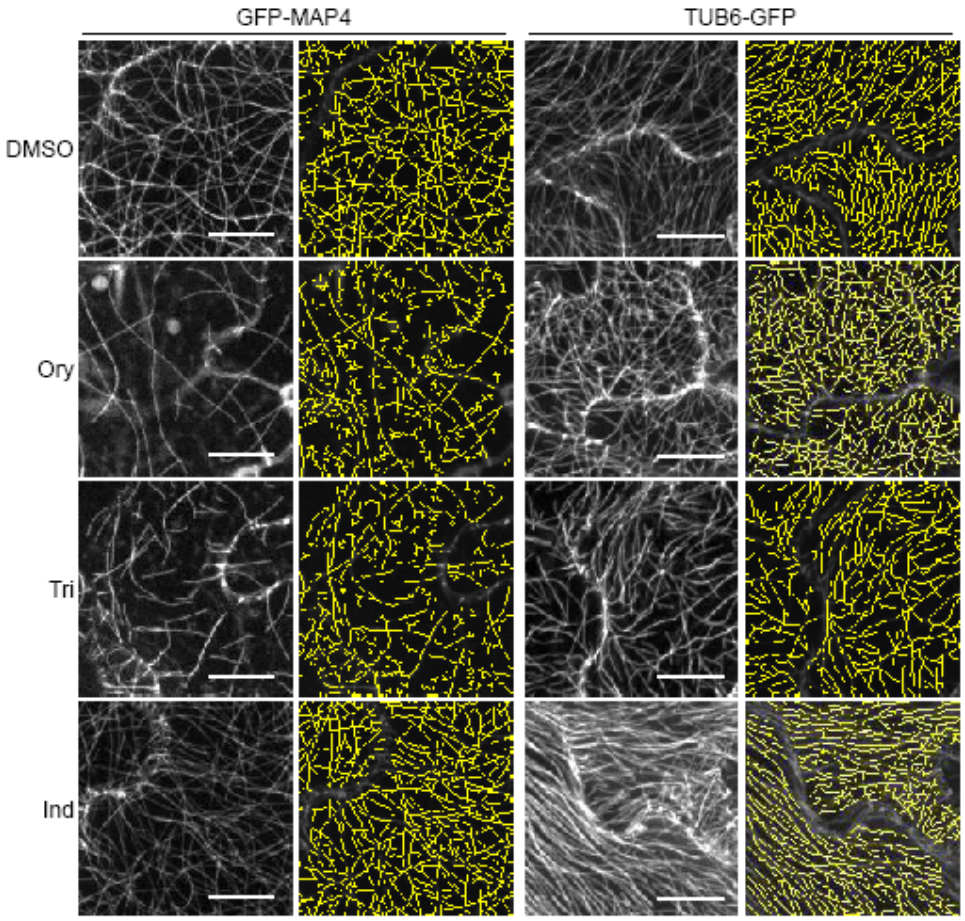

Figure 3: Quantification of the effects of chemicals C1-C6, indaziflam, trifluralin and oryzalin on microtubule patterns by CellArchitect. Box plots: boxes indicate the boundaries of the upper and lower quartiles with bars indicating maximum and minimum values (excluding outliers which are shown by circles), the black bar identifies the median. Different letters indicate significantly different values at $p < 0.05$ (ANOVA post-hoc Tukey).

This article is protected by copyright. All rights reserved.

Accepted Article

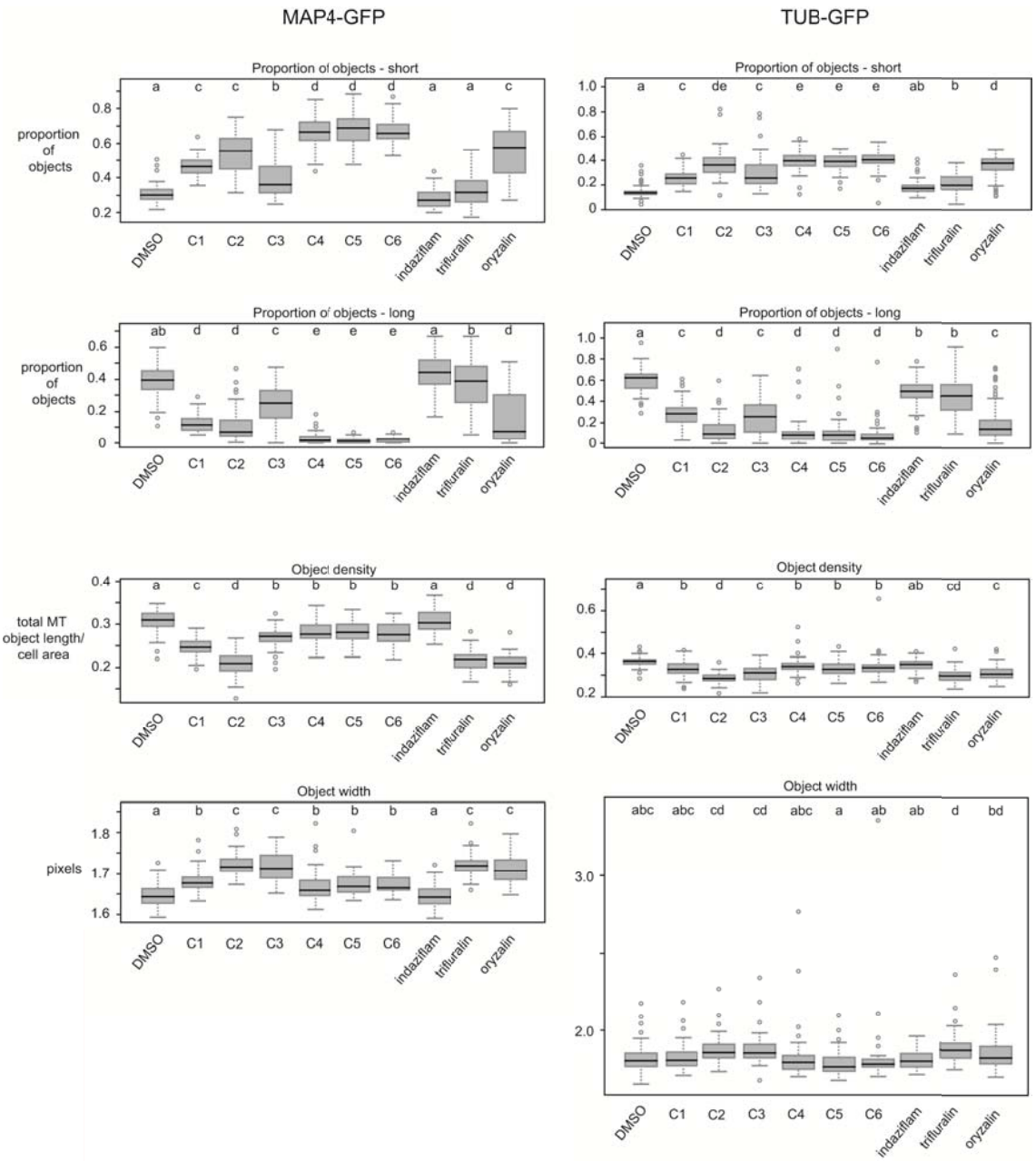

Figure 4: The effects of unknown chemicals C1-C6 on microtubule patterns in Arabidopsis cotyledon epidermal pavement cells. Microtubules are marked by stable expression of GFP-MAP4 and TUB6-GFP. Microtubule pattern detection by CellArchitect is shown with colour coding according to object length: green: short; medium-short; orange: medium-long; red: long. Scale bars are 15 μm.

This article is protected by copyright. All rights reserved.

Accepted Article

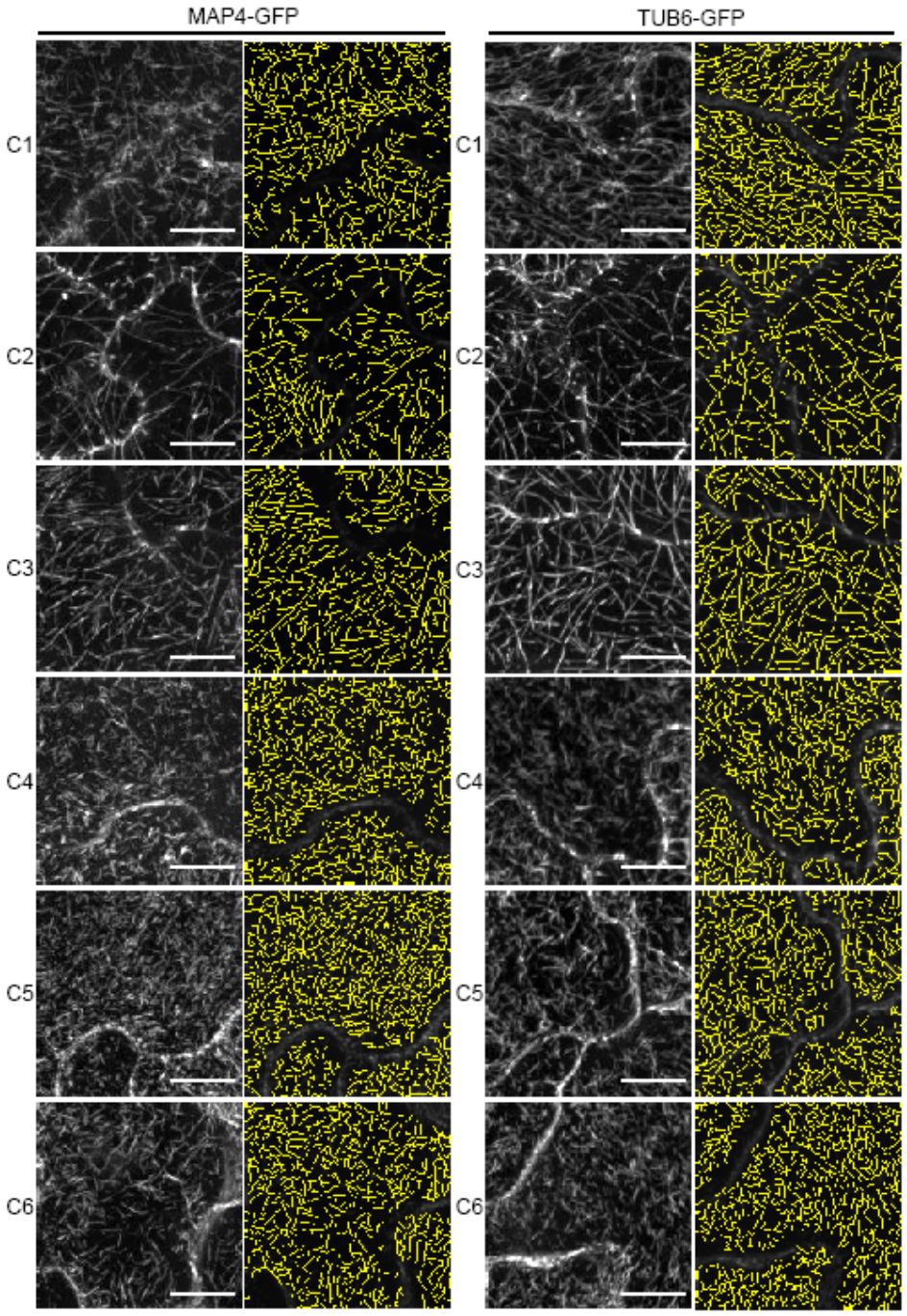

Figure 5: Quantification of the effects of chemicals C1-C6, indaziflam and trifluralin on endomembrane markers mRFP-ARA7/RabF2b (endosomes), VTI12-YFP (*trans*-Golgi network) and SYP32-YFP (Golgi) by EndomembraneQuantifier. Box plots: boxes indicate the boundaries of the upper and lower quartiles with bars indicating maximum and minimum values (excluding outliers which are shown by circles), the black bar identifies the median. Different letters indicate significantly different values at $p < 0.05$ (ANOVA post-hoc Tukey).

This article is protected by copyright. All rights reserved.

Accepted Article

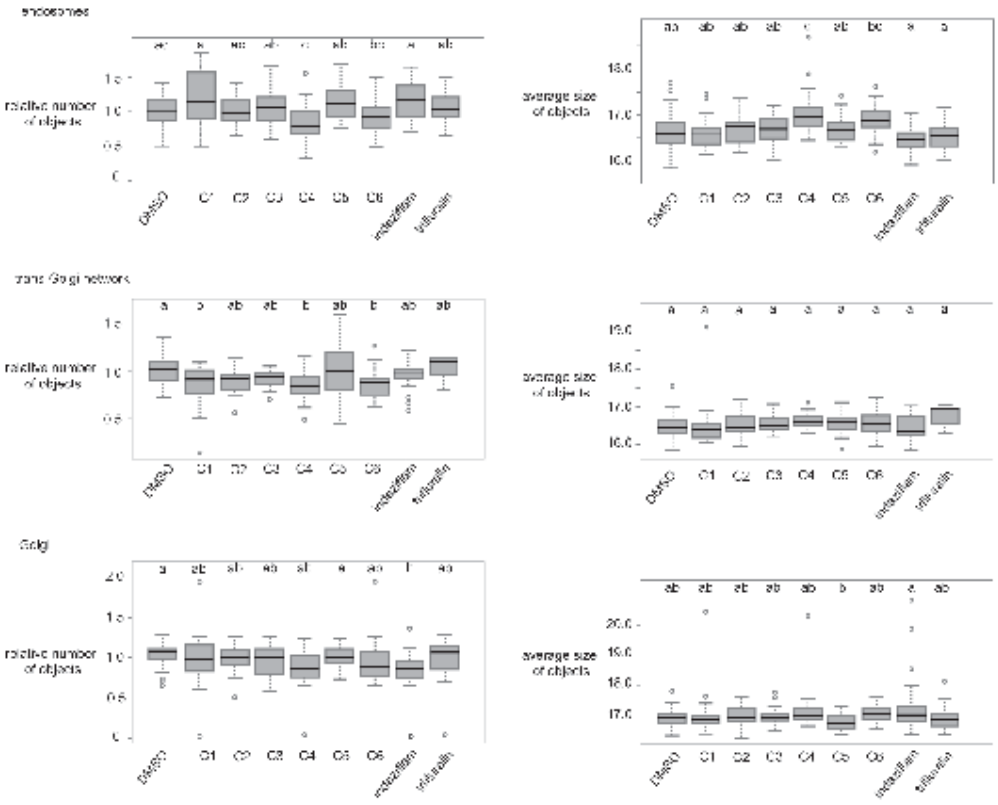

This article is protected by copyright. All rights reserved.